Chalcogenide Letters Vol. 22, No. 2, February 2025, p. 151 - 166

Effect of porosity of mesoporous silicon substrates on CdS thin films deposited by chemical bath deposition

F. Saker[a,*], L.Remache[a], D. Belfennache[b], K. R. Chebouki[a], R. Yekhlef[b]
[a]*Laboratory of Materials and System Structure and their Reliability, Oum El Bouaghi University, Oum El Bouaghi,04000, Algeria*
[b]*Research Center in Industrial Technologies CRTI, P.O. Box 64, Cheraga, 16014 Algiers, Algeria*

In this work the chemical bath deposition (CBD) method was used to synthesize Cadmium sulphide (CdS) thin films on glass, silicon (Si), and porous silicon (PSi) substrates. The PSi substrates were prepared by an electrochemical etching method using different current densities at constant etching time of 5 minutes. The CdS thin films were characterized using the X-ray diffraction (XRD), scanning electron microscopy (SEM), atomic force microscopy (AFM), optical transmittance spectroscopy in the Uv visible range, and electrical characterization (I–V characteristics). The obtained results demonstrated that the morphology of the deposited materials was influenced by the porosity of the PSi substrates. The average crystallite dimensions for CdS/glass and CdS/Si were determined to be 46.12 nm and 23.08 nm, respectively. In CdS/PSi structures, the average value of the grain size decreases with increasing porosity. The smallest one is obtained for the CdS/PSi structure with 70% porosity, amounting to 11.55 nm and the smallest value is also for the mean the RMS (Root-Mean-Square) value 18.83 nm. The measured current-voltage characteristics in coplanar structure on the CdS/PSi/Si sample showed that the photocurrent of the CdS/Si structure is of 3.17 μA and increases up to 600 μA for the CdS/PSi/60% structure.

(Received November 11, 2024; Accepted February 10, 2025)

Keywords: Chalcogenide semiconductors, Porous silicon, CdS, Thin film, CBD

1. Introduction

Semiconductors have attracted considerable attention from researchers in different fields because of their excellent performance capability in optics, electronics, and photonics [1-4]. Historically, metal oxide semiconductors have been recognized to be feasible for optoelectronic devices. Metal chalcogenide nanostructures have also emerged as promising materials due to their specific characteristics and advantages compared with other nanomaterials, related to their low cost, chemical stability, simplicity of synthesis, and superior optoelectronic performance [5].

Cadmium sulfide (CdS) is recognized as one of the most extensively studied materials within the category of chalcogenide semiconductors. Its direct intermediate band gap, which is approximately 2.5 eV, in conjunction with a relatively low work function, high refractive index, and remarkable thermal and chemical stability, renders it highly appealing for various applications [6]. Cadmium sulfide (CdS) has diverse applications across numerous fields, including solar cells, light emitting diodes (LEDs), photodetectors, waveguides, and lasers [6]. Importantly, improvements in synthesis methods have facilitated the precise fabrication of nanostructured CdS with customized dimensions and forms. These nanostructures exhibit intriguing properties such as laser cooling, Franz-Keldysh effect, and quantum confinement due to surface depletion [7,8]. With most reviews copiously focusing on growth techniques and mechanisms [9, 10], cadmium sulfide thin films could be synthesized using PVD and solution growth deposition methods. Indeed, several conventional methods such as chemical bath deposition, sputtering, thermal evaporation, MBE, sol-gel processes, spin coating,

---

[*] Corresponding authors:fatima.saker@univ-oeb.dz

https://doi.org/10.15251/CL.2025.222.151

electrodeposition, and screen printing have been widely utilized for CdS thin film deposition [11,12]. Among them, the chemical bath deposition is worth mentioning since it's a very user-friendly technique, offering several economic advantages coupled with its steady performance, thereby making it widely popular among other thin film deposition methods. Moreover, the advantage with CBD is the capability for large-area deposition and low-temperature deposition of CdS thin films [13]. The crystallinity of the CdS thin films prepared by CBD is superior, with a lower defect density compared to other alternative deposition techniques. These films exhibit a well uniformity, granularity, continuity, and smoothness, presenting negligible surface roughness [11]. The development of films is dependent on the influencing factors of deposition, including bath concentration, solution temperature, pH, deposition duration, and substrate characteristics [14-16]. The nature and properties of the substrate used will influence the microstructure and adhesion of the resultant film. Thus, the choice of substrates can considerably enhance or alter the general properties of the final products [17].

The use of of silicon in various technological fields has attracted the attention of many researchers due to its distinctive properties [18-20]. On the other hand, porous silicon becomes a promising material for detection applications because of many reasons: morphology, large specific surface area, low energy consumption, compatibility with silicon-based technologies [21, 22]. In addition, various morphological and structural properties of this material can be achieved in a localized manner by low-cost electrochemical process, which can be integrated on silicon through microtechnological processes [21]. PSi sensitivity is influenced by the morphological properties of pores, such as pore diameter, degree of homogeneity, surface roughness, and layer thickness [23]. Furthermore, its large specific surface area makes it more reactive than bulk silicon. In this context, the variation of porosity can influence the surface roughness and the specific surface area of the PSi substrate. Rahmani et al. [24, 25] show that increases in porosity results in an increase in roughness and also uncovers the evolution of PS nanocrystallites. On the other hand, many works shown that the variation in porosity in the range of 50 to 70% yields to a high average specific surface area around 600 cm^2/m^3. [26, 27]. In order to manufacture high-performance photodetectors, many studies have reported the improvement in the performance of detector when prepared on porous silicon [23]. Another more attractive way is to deposit nanoparticles of materials into the PSi matrix, hence improving the electrical properties of the elaborated layers and produces sensors with higher and faster response [28]. In the realm of porous silicon, various materials like ZnO, ZnS, TiO_2, and more can be seamlessly integrated into the matrix [29, 30]. Hasoon*et al.* [31] has achieved the deposition of nanostructured CdS thin films on the PSi matrix by the vacuum thermal evaporation method. Sara *et al.* [32] adopted a different path, by preparing a CuS/PSi heterojunction photodetector using the chemical spray pyrolysis route. Khashan [33] succeeded in ZnO nanoparticles incorporating into PSi matrix through chemical method. Similarly, Habubi investigated the response improvement of PSi photodetectors when incorporated with CdSe nanoparticles prepared via laser ablation [34]. Li *et al.* [35] conducted an interesting study on the electronic properties of the CdS/Si nano-hetero structure prepared via chemical bath deposition technique on a silicon nanoporous pillar array. Perillo *et al.* [36] demonstrated the photoresponse performance of CdS thin films, deposited by CBD on glass, through low-temperature thermal treatment.

The novelty of this study is to examine the influence of the porosity of mesoporous silicon substrates on CdS thin films deposited by chemical bath deposition. By comparing the structural, morphological, and optical properties of the CdS layers on the PSi substrate with those on CdS/Si and CdS/glass structures.

2. Materials and methods

2.1. Porous silicon formation

The PSi layers were prepared by the anodization of p-type Boron-doped (100) oriented mono-crystalline silicon (CSi) wafers, with resistivity of 0.015−0.018 Ω cm and thickness of 250 − 300 μm, in a solution composed of hydrofluoric acid and ethanol. The unpolished face of the silicon served as the anode, while a platinum electrode served as the cathode. The silicon wafers were treated before the anodization process by rinsing them with a 2% hydrofluoric acid solution. Electrolyte preparation was performed by mixing 40% hydrofluoric acid with 99.98% ethanol in a 1:1 volumetric ratio. A single-cell configuration was used, connected to a Keithley 2400 generator. The porous layers were prepared at various current densities, namely 5, 30, 60, and 100 mA/cm^2 during 5 min at room temperature, where the porosity of PSi was found to be around 37%, 53%, 60%, and 70%, respectively. Finally, take out the samples and clean them by ethanol and then dry using a hair dryer.

2.2. CdS Synthesis

Glass, Si and PSi substrates were used to deposited thin films using chemic CBD technique. The CdS solution in this work is made by mixing cadmium sulfate ($CdSO_4$), ammonia (NH_4OH), thiourea ($CS(NH_2)_2$), and de-ionized water (DIH_2O). The samples were soaked at 50° for 60 minutes with magnetic stirring in this solution. After that, the samples were retrieved from it, collected, cleaned with de-ionized water, and dried in the air with a hair drier. All the films were yellowish in color, homogeneous, and well-covered on the entire surface. In this study, different structures were considered: CdS nanoparticles deposited on glass (CdS/glass), on silicon (CdS/Si), and on porous silicon prepared at room temperature with current densities of 5 mA/cm^2 (CdS/P Si 37%), 30 mA/cm^2 (CdS/PSi 53%), 60 mA/cm^2 (CdS/PSi 60%), and 100 mA/cm^2 (CdS/P Si 70%). The crystallographic structure of the prepared samples was investigated by an ARL-EQUINOX100 X-ray diffractometer using CuKα1 radiation at an operation current of 40 mA and voltage of 40 kV. The optical transmittance of CdS thin films was measured by a JacsoV-30 UV-visible spectrophotometer. The surface morphology of the films was investigated by a scanning electron microscope (SEM) JEOL JSM-7001 F. The atomic percent composition of the thin films was evaluated by energy dispersive X-ray (EDX) analysis.

3. Results and discussions

3.1. Structural characterizations

Fig.1 shows the X-ray diffraction spectra for the same current densities described above for CBD-CdS films synthesized on glass, silicon, and PSi substrates. The recorded diffraction patterns confirm that indeed the deposited CdS films are polycrystalline in nature. More precisely, it was observed that among all peaks, the intensity of the (002) peaks was higher; hence, the crystallites exhibit a preferential orientation along the (002) plane perpendicular to the substrate. This observation is in good agreement with the LCDD No. 01-083-5246 that shows a hexagonal (Wurtzite) crystalline structure [37]. Other peaks correspond to reflections from the planes (110) and (112). Such reflections indicate a hexagonal CdS film. Another extra reflection in CdS/Si, CdS/PSi37%, CdS/PSi53%, and CdS/PSi60% attributed to cubic CdS phase (200) also appears beside the hexagonal one. Most frequently, XRD studies of PVD deposited CdS thin films showed that they have a dominant hexagonal structure, and solution growth deposited CdS films showed a dominant hexagonal or dominant cubic or a mixed structure [38–43]. Hexagonal CdS structure is recommended due to its higher stability regarding the cubic one [44].

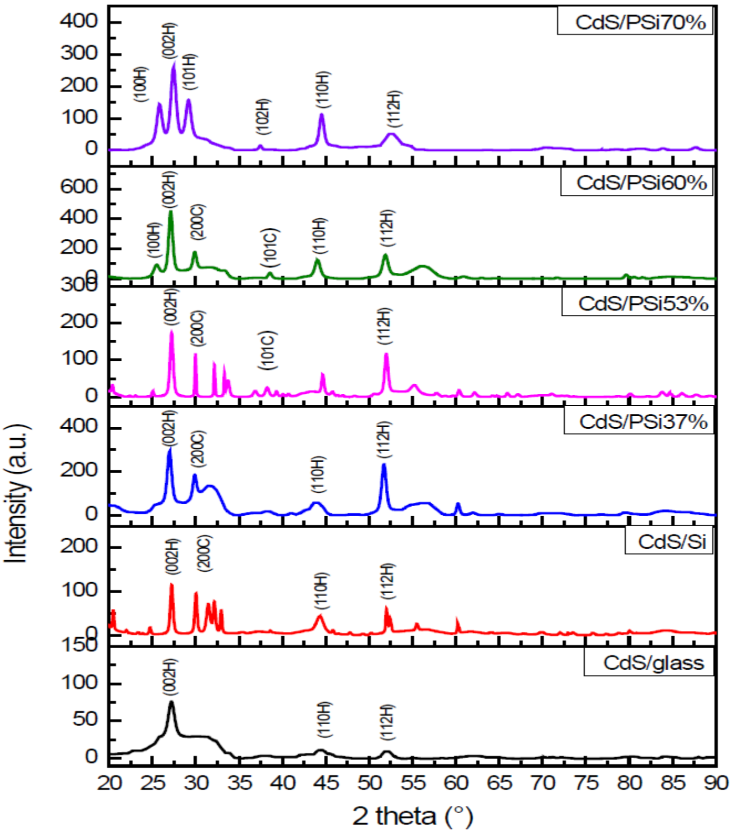

Fig. 1. XRD spectra of CdS nanoparticles deposited on glass, silicon and porous silicon.

The distinctive peaks (101) and (200), originating from the cubic metastable phase, underwent a remarkable transformation within the domain of the hexagonal stable phase. Specifically, (101) evolved into (102), while (200) transmuted into (101). This interesting observation revealed that CdS/PSi70% has a unique single-phase hexagonal structure, which distinguishes it from the other examined samples. Remarkably, Haque *et al.* [45] obtained similar results to ours but by pre-deposited film heating. In our study we achieved the conversion from a mixed phase to the hexagonal stable phase by manipulating the porosity of the PSi substrate. Additionally, in CdS/PSi(60%) and CdS/PSi(70%) structures, we noted the emergence of an additional peak corresponding to the (101) plane within the hexagonal phase. Further examination of the diffraction spectra shed light on distinct characteristics. When the CdS film was deposited on a glass substrate, the diffraction peaks exhibited reduced intensity, suggesting their lower crystallinity. This result can be attributed to the amorphous nature of the glass substrate [46]. In contrast, the diffraction peaks for the CdS films deposited on PSi substrate became more pronounced and narrower, indicating the film's crystallinity improvement [47]. It is well known that the formation energy required for crystallization is higher when dealing with amorphous substrates like glass compared to crystalline substrates, which promote nucleation. This fundamental distinction explains the lower crystallinity observed in the CdS/glass structure. Notably, the CdS film grown on the PSi substrate exhibit superior crystallinity compared to the other substrates, as demonstrated in Figure 1. This crystalline superiority makes it a remarkable specimen deserving of attention and further exploration.

With the application of Bragg's diffraction condition, the calculation of interplanar spacing (d) for different planes across all XRD patterns is possible [48].

$$2\, d \sin\theta = n\, \lambda \qquad (1)$$

Where:
Here, θ is the angle of diffraction, n gives the order of diffraction, and κ is the wavelength of X-ray radiation from CuKα (λ = 0.154 nm).
Using Bragg's formula for the hexagonal system [49], the 'a' and 'c' lattice parameters are determined from the position of the peaks.

$$\frac{1}{d^2} = \frac{4}{3}\frac{(h^2+hk+k^2}{a^2} + \frac{l^2}{C^2} \tag{2}$$

The minor deviation from the standard values can be attributed to the strain induced in these samples because of excess Cd interstitials or S vacancies [49].
The crystallite size can be simply determined using the Scherer formula [49] as follows:

$$D = \frac{k\lambda}{\beta cos\theta} \tag{3}$$

Where:
β represents the full width at half maximum (FWHM in radians) of the peak, adjusted for instrumental broadening.
θ is the diffraction angle measured in radians
k : Scherer constant (k = 0.9)
λ: Wavelength of X-ray.

The lengths are expressed in [˚A] and the angles in radians.

The strain values ϵcan be calculated using the following formula [32]:

$$\varepsilon = \frac{\beta cos\theta}{4} \tag{4}$$

The density of dislocations δ is determined by the Williamson and Smallman's relation [50]:

$$\delta = \frac{1}{D^2} \tag{5}$$

Table 1 presents the lattice parameter values obtained. These values have a good agreement with the published data.

Table 1. Structural parameters for the strongest peaks of CdS nanoparticles deposited on different substrates

Substrates	Structure	(hkl)	I / I_0	2θ (°)	$d_{spasing}$(A°)	Lattice constant
CdS/ glass	Hex	(002)	100	26.6352	3.3417	
	Hex	(110)	14.76	44.2537	2.0467	a =4.0890
	Hex	(112)	12.07	52.4457	1.7447	c =6.6936
CdS/Si	Hex	(002)	100	27.2090	3.2775	
	Cub	(200)	82.61	30.0070	2.9779	a =4.1986
	Hex	(110)	37.46	44.2794	2.0456	
	Hex	(112)	52.35	51.9987	1.7586	c =6.5550
CdS /PSi37%	Hex	(002)	100	26.8596	3.3193	
	Cub	(200)	62.79	29.7193	3.0061	a =4.1746
	Hex	(110)	19.46	43.9789	2.0589	
	Hex	(112)	78.91	51.7355	1.7670	c =6.6384
CdS /PSi53%	Hex	(002)	100	27.2016	3.2784	
	Cub	(200)	68.84	29.9541	2.9831	a= 4.1726
	Hex	(110)	34.58	44.6292	2.0304	
	Hex	(112)	67.74	51.9526	1.7601	c= 6.5568
CdS /PSi60%	Hex	(100)	19.79	25.4144	3.5047	
	Hex	(002)	100	27.0974	3.2907	a =4.1562
	Cub	(200)	39.66	29.9875	2.9798	
	Hex	(110)	27.66	44.0521	2.0556	c =6.8516
	Hex	(112)	35.24	52.0017	1.7585	
CdS /PSi70%	Hex	(100)	54.50	25.8233	3.4501	
	Hex	(002)	100	27.4168	3.2531	a = 4.0832
	Hex	(101)	60.68	29.2907	3.0491	
	Hex	(110)	79.00	44.4943	3.0362	c =6.5063
	Hex	(112)	35.30	52.0950	1.2792	

Data from X-ray diffraction on FWHM, crystallite size, strain, and dislocation density concerning CdS thin films deposited onto various substrates are presented in Table 2. From the results obtained, crystallite size decreases in films grown on Si and PSi substrates. The smallest value of crystallite size was measured in the largest porosity Psi substrate (70%). Additionally, the strain and dislocation density values are lower in the case of films deposited on glass substrate. By comparing the diffraction pattern of films deposited on glass and of those deposited on Si and PSi substrates for different current densities, we can observe that most peak diffraction shift towards the bigger angles. It is well known that the deformation due to planar stress causes the shift in XRD peaks. Therefore, the values of strain calculated in Table 2 confirm the fact.

Table 2. X-ray diffraction data of 2θ, full width half maximum (FWHM), crystallite size, strain and dislocation density of (002) plan for CdS thin films deposited on glass, silicon and PSi substrates.

Substrates	2θ (°)	FWHM (°)	D(nm)	$\varepsilon .10^{-3}$	$\delta .10^{-3}$ (nm^{-2})
CdS/ glass	26.6352	0.1771	46.120	0.751	0.470
CdS/Si	27.2090	0.3542	23.088	1.501	1.875
CdS /PSi37%	26.8596	0.3542	23.071	1.502	1.878
CdS /PSi53%	27.2016	0.4133	19.786	1.752	2.554
CdS /PSi60%	27.0974	0.5314	15.385	2.253	4.224
CdS /PSi70%	27.4168	0.7085	11.554	3.002	7.490

3.2. Morphological study:

Fig. 2 shows the SEM images of CdS thin films deposited on glass (a) and on silicon (b) substrates.

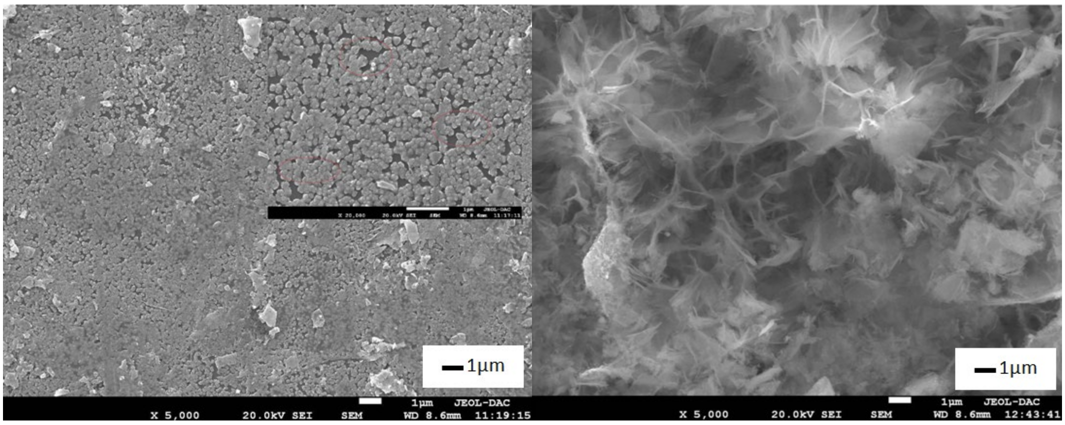

(a) *(b)*

Fig. 2. SEM images of (a) CdS/glass, (b) CdS/Si.

CdS/glass sample structure show the presence of compact globular structures owing spherical and hexagonal shapes. These structures are composed of nanoparticles that maintain a uniform size. However, careful observation reveals the existence of voids between the grains, indicating incomplete growth of CdS thin films. It is plausible that the smooth nature of the glass substrate hampers the perfect development of CdS thin films.

In contrast, the SEM image of the CdS/Si structure portrays the formation ofmicro-flowers, micro-sheets, and micropores on the surface. These micro-features create an environment conducive to the formation of non-spherical nanoparticles within the micropores. This distinct morphology of the nanoparticles can be attributed to the intrinsic roughness of the silicon surface, which provides favorable conditions for the growth of non-spherical CdS nanoparticles in the recesses of the micropores. Moreover, an interesting discrepancy becomes evident when comparing the particle density of the CdS/Si thin films to that of the CdS/glass structure. Remarkably, the particles in the CdS/Si thin films appear to be more densely packed compared to those in the CdS/glass structure. This disparity in particle density becomes visually apparent in Figure 3, which depicts the morphologies of both the porous silicon (PSi) and CdS/PSi structures. This distinction can be ascribed to the distinctive characteristics of the silicon substrate, which likely facilitate a more compact deposition of CdS thin films.

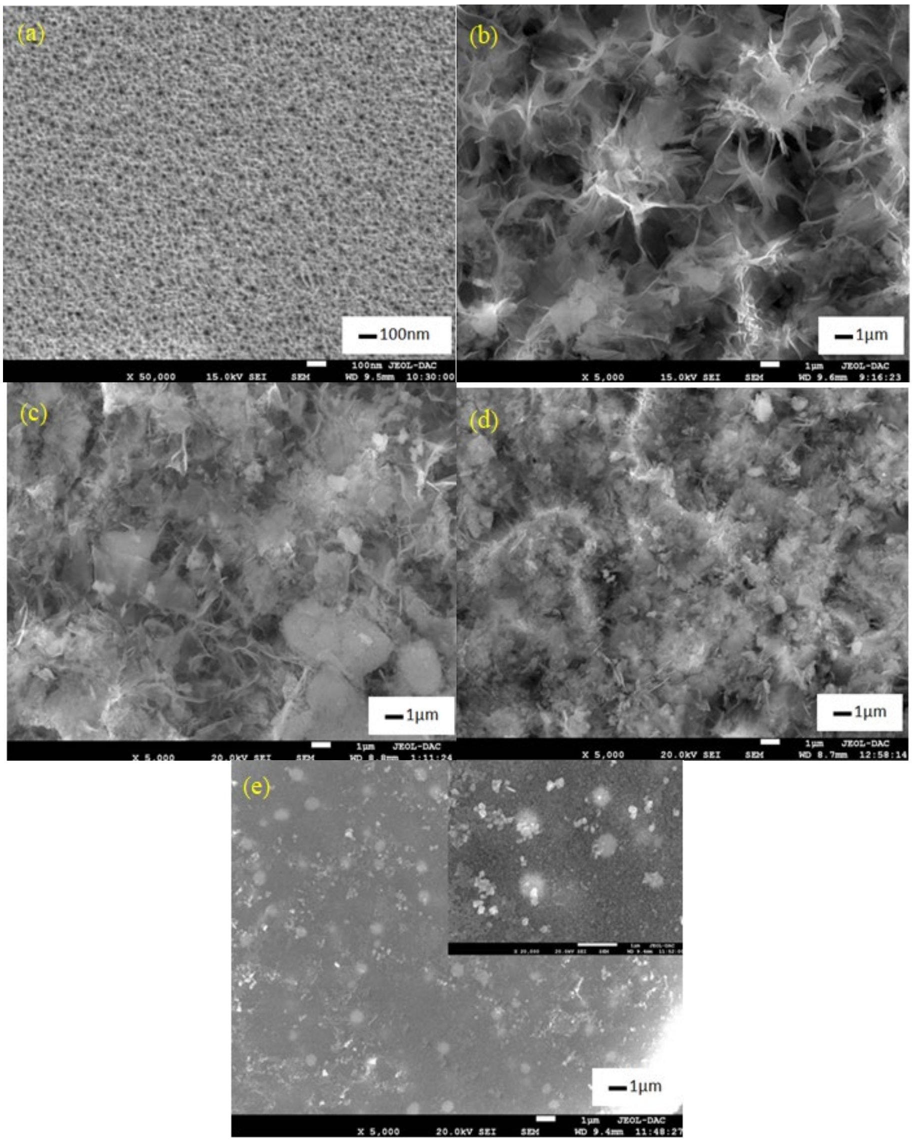

Fig. 3. SEM images of (a) PSi60%, (b) CdS/PSi37%, (c) CdS/PSi53%, (d) CdS/PSi60%, and (e) CdS/PSi70%.

Figure 3 (a) illustrates the SEM image of the porous silicon matrix. The surface clearly consists of semi-circular shaped pores, which are distinctive by their uniform distribution and great density. The size of these pores falls within the range of 20 to 25 nm. Regarding the CdS/PSi structures, the SEM observation of the CdS/PSi37% structure (Fig. 3 (b)) exhibits the formation of micro-flowers, which subsequently generate pores with diameters on the scale of a few micrometers. These pores undergo widening and deepening due to the porous nature of the silicon substrate and the heightened surface roughness. A transition in the sample morphology is observed in the CdS/PSi53% structure (Fig. 3 (c)), where the micro-flowers and pores partially disappear, leading to the emergence of micrometric plates on the surface. Additionally, spherical nanoparticles appear and tend to aggregate, retaining their shape and forming macroscopic hierarchical masses. As the porosity of the silicon substrate increases to a specific threshold (around 60% (Fig 3 (d)), the characteristic flower-like morphology completely vanishes. Instead, of these two distinct types of nanoparticles appear. Firstly, nano plates with dimensions spanning from 300 nm to 1 µm are observed. Secondly, spherical nanoparticles with a striking white appearance reminiscent of snowballs are formed. Notably, upon reaching 70% porosity in the silicon substrate (figure 3 (e)), the SEM image reveals the complete disappearance of micro-flowers and micro-plates followed by the formation of spherical nanoparticles with dimensions ranging from 10 nm to 50 nm, with a uniform distribution across the entire surface. Furthermore, the agglomeration of nanoparticles with identical dimensions leads to the formation of microspheres with diameters between 500 and 700 nm. Additionally, microspheres characterized by inhomogeneous and low-density structures also emerge through the agglomeration of nanoparticles of similar dimensions.

In summary, the SEM analysis offers valuable information regarding the unique morphological characteristics observed in the CdS/glass and CdS/Si configurations. In the CdS/glass structure, spherical nanoparticles form globular structures, whereas the CdS/Si structures are composed of micro-flowers, micro-sheets, and non-spherical nanoparticles within micropores. Additionally, the CdS/Si thin films exhibit a greater particle density compared to the CdS/glass structure. Furthermore, the investigation of CdS/PSi structures evolves from micro-flowers and pores to micrometric plates and aggregated spherical particles.

3.3. Compositional analysis

To determine the element composition and the ratio of atomic percentage of different elements in CdS thin films prepared by CBD, we have used energy-dispersive X-ray (EDX) analysis .In Figure 4, we have reported the recorded EDX spectra in different samples. As seen, high peaks assigned to Sulfur (S) and Cadmium (Cd) element are present in whole spectra confirming the formation with a good purity of CdS thin films. However, we noticed that the percentage of Cd and S elements is higher in the case of the CdS/PSi structure than in the other ones, reflecting better crystallization of CdS on porous silicon.

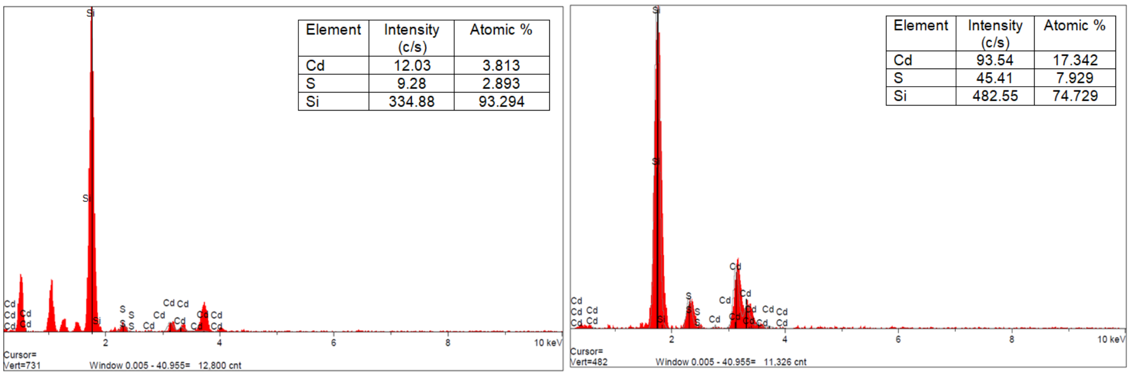

Element	Intensity (c/s)	Atomic %
Cd	12.03	3.813
S	9.28	2.893
Si	334.88	93.294

Element	Intensity (c/s)	Atomic %
Cd	93.54	17.342
S	45.41	7.929
Si	482.55	74.729

(a) *CdS/glass* (b) *CdS/Si*

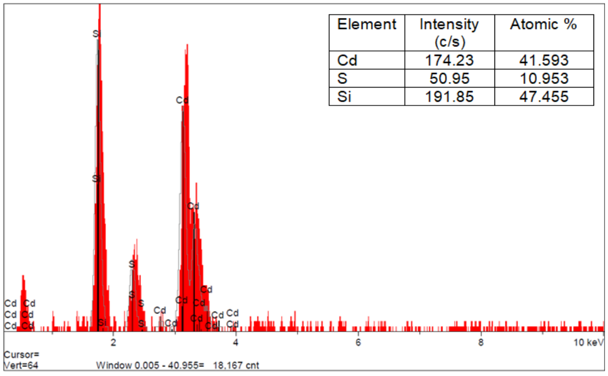

Element	Intensity (c/s)	Atomic %
Cd	174.23	41.593
S	50.95	10.953
Si	191.85	47.455

(c) *CdS/PSi60%*

Fig.4.EDX spectrum of nanocrystalline CdS thin films.

3.4. Atomic force microscopy (AFM) characterization

The roughness of thin films is a important parameter to study and determine their properties more accurately. In order to better measure the roughness of our samples, we based on the measurement of the factor of roughness RMS to the surface of the WSxM software [51].

AFM analysis was carried out to observe the surface morphology of mesoporous silicon substrates on CdS thin films deposited by chemical bath deposition.

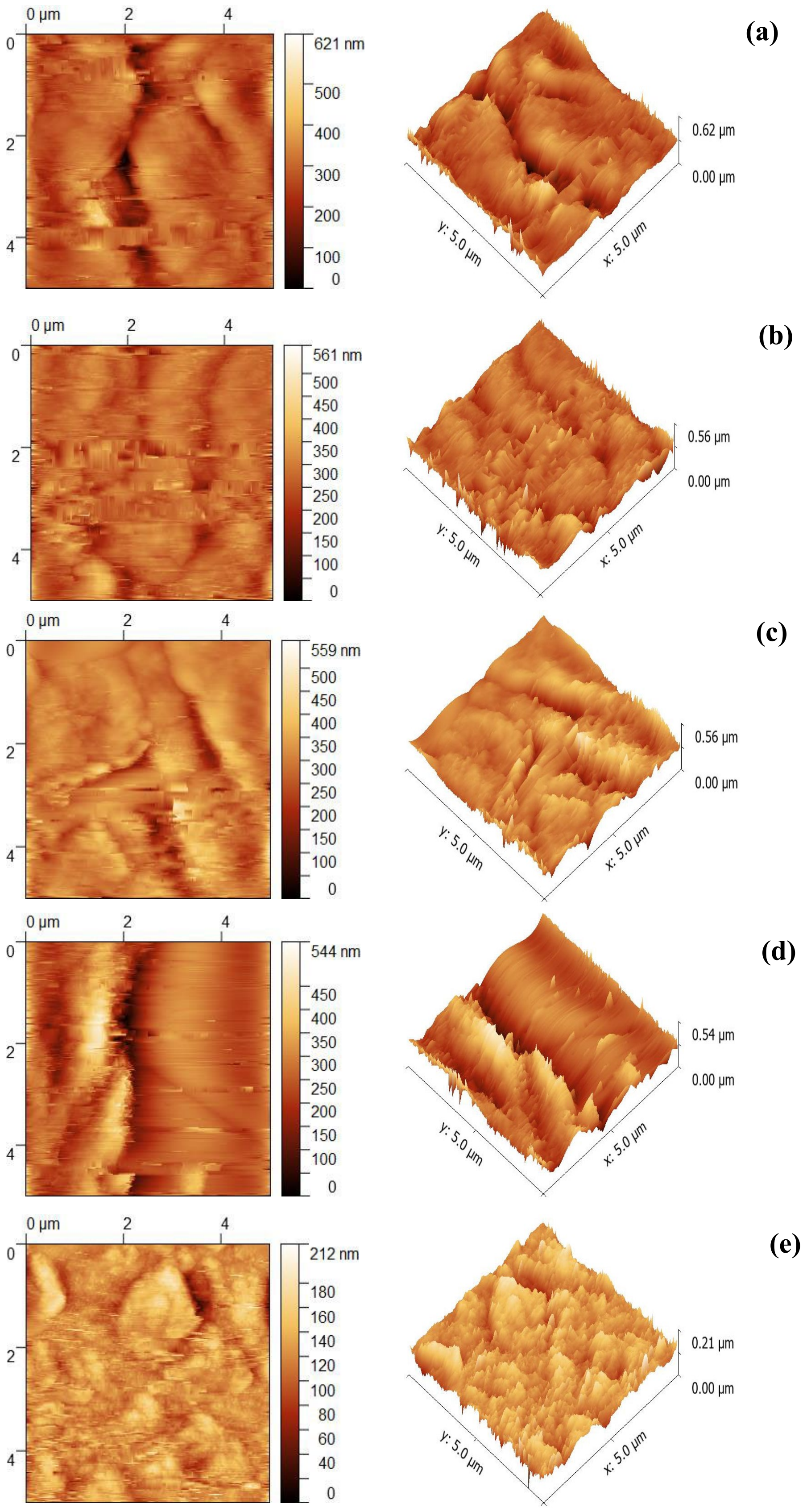

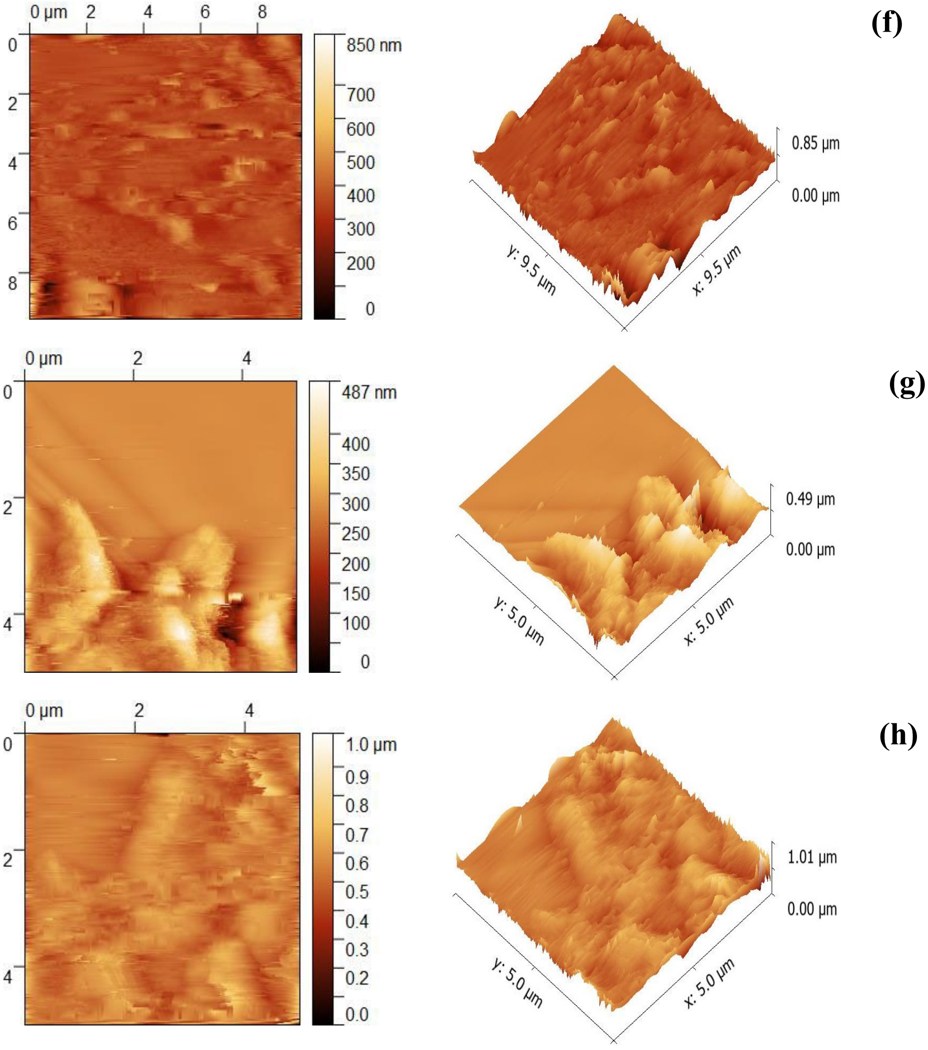

Fig.5 AFM micrographs of: (a) CdS/PSi 37% , (b) CdS/PSi 53%, (c) CdS/PSi 60%, (d)CdS/PSi 60 bis% , (e) CdS/PSi 70%, (f) CdS/glass, (g) CdS/Si, (h) CdS/Si bis.

Fig. 5 shows the topographies of the CdS/Si thin films, the 2D AFM image of films displays presence of elongated grains with different sizes and the 3D AFM image confirms formation of agglomerated grains oriented upward. The results of the analysis indicate the presence of islands with different shape, size and number. This is well described according to the “Volmer-Weber” mode the binding energy between metal ad-atom and substrate atoms is smaller than the binding energy between metal ad-atoms themselves, which leads over of a 3D metal forming on substrate. Fig. 5(e) shows a large number of islands covering irregularly the surface of the films, explaining the rough surface and the RMS (Root-Mean-Square) value which equals 18.83 nm. However, for the CdS/Si Fig 5 (g) it was clearly observed a diminution in the number and the size of CdS islands smoothly dispersed on the surface, leading to low roughness than the pulsed method. The RMS values are summarized in the table 3. Moreover, some holes, that are due to the hydrogen bubbles release on the surface of the deposits, are observed; thereby inhibiting the deposition rate of the alloy in some surface sites that which lead to the appearance of holes observed on images. By way of comparison, Raid A. Ismail*et al.* [52] have obtained a roughness found rms values of 11and 7 nm for CdS/Si prepared by spraypyrolysis technique.

Table 3. The RMS values for various samples

Sample	RMS (nm)
CdS/PSi 37%	54.93
CdS/PSi 53%	37.26
CdS/PSi 60%	43.11
CdS/PSi 60 bis%	64.32
CdS/PSi 70%	18.83
CdS/glass	43.77
CdS/Si	40.96
CdS/Si bis	54.40

3.5. Optical characterization

In order to study the optical gap of the CdS samples, the optical transmittance spectroscopy, in the Uv visible range, of thin film deposited on glass is used. Figure 6 illustrates the variations in transmittance with respect to wavelength. The spectrum exhibited absorption edges at around 500 nm, which indicated the existence of the optical band gap of the CdS thin film. The average transmittance obtained within the visible spectrum is about 55%. It is worth noting that the reduced transmittance of the deposited film could be attributed to the surface roughness resulting from the morphology of clustered CdS thin films.

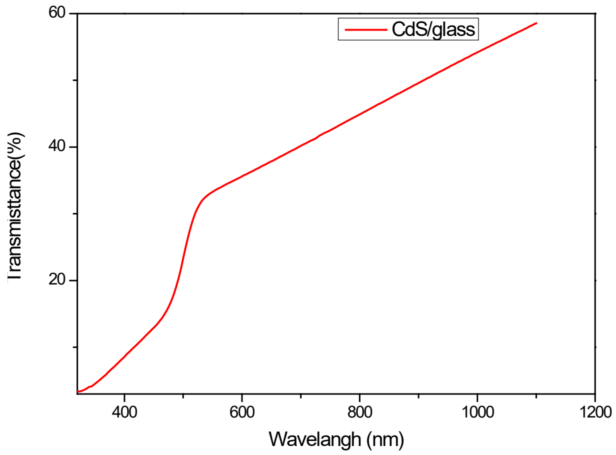

Fig. 6. Optical transmittance spectrum of CdS thin film.

The relationship between the energy of the photon and the optical absorption coefficient (α) for direct transitions is expressed by the following Tauc equation [53]:

$$\alpha(h\nu) = (h\nu - E_g)^{\frac{1}{2}} \tag{6}$$

Where: A: Independent energy constant, Eg: Optical band-gap of semiconductor (eV), hv: Photon energy

In figure 7, we have plotted $(\alpha h\nu)^2$ as a function of the energy of the photon. The optical film's band gap was estimated from the intercept of the linear part of $(\alpha h\nu)^2$ up with the x-axis. The obtained energy band gap of CdS thin film deposited on glass is 2.3 eV. This result is in good agreement with that published in the literature [54].

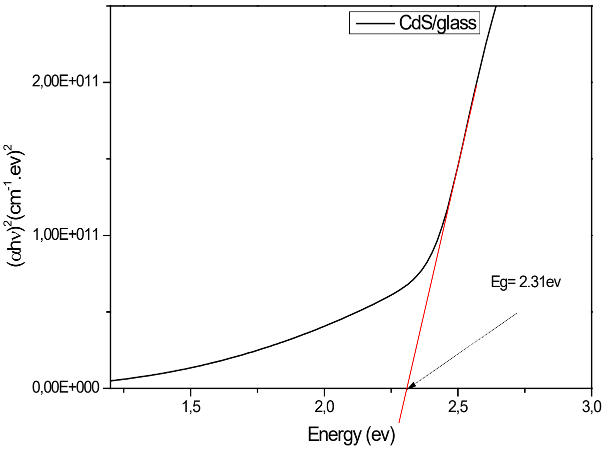

Fig. 7. Determination of the energy gap for the CdS thin film.

3.6. Electrical characterization

For the film's electrical characterization, we have measured DC conductivity in a coplanar structure. Two circular silver (Ag) electrodes were placed on the surface to perform electrical conductivity measurements at a distance of 5 mm (Figure 8a). The choice of the distance between the Ag electrodes was intended to guarantee the flow of electric current, taking into account the geometric properties of the electrical contacts used in previous studies [55].

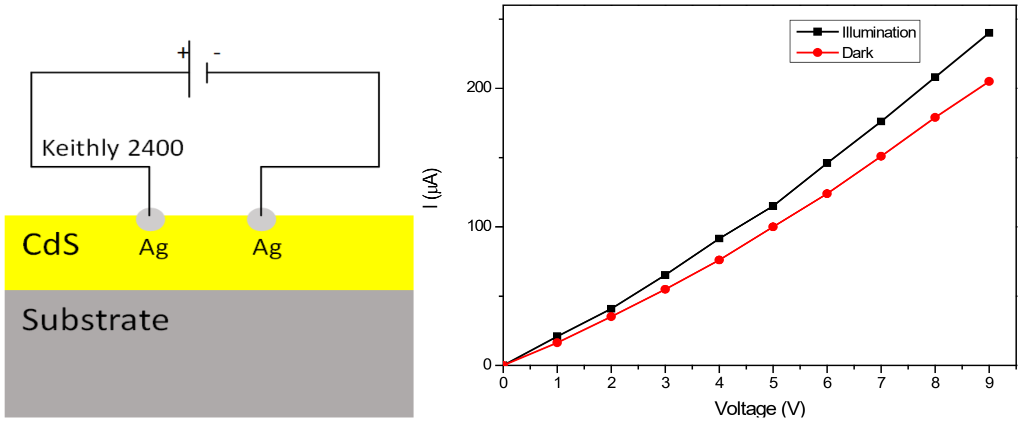

(a) Structure used for I-V characterization *(b) CdS/PSi70%*

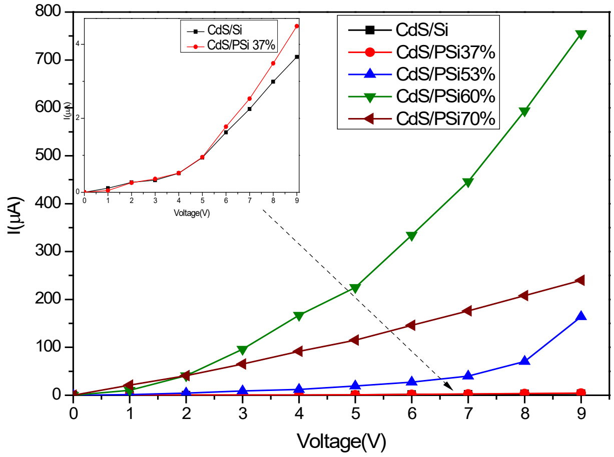

(c) CdS/Si and CdS/PSi structures under illumination

Fig. 8. I–V characteristics.

In Figure 8b, we have plotted the recorded current-voltage (I-V) characteristics, measured in total darkness and under illumination. It is evident that as the applied voltage increases, the current values of the CdS films increase significantly, both in dark and illuminated conditions. Moreover, the measured current in illuminated condition is larger than in dark one, this is attributed to the photonconductivity of the prepared CdS films; this suggests their possible application as photodetector. The CdS/Si, CdS/PSi37%, CdS/PSi57%, CdS/PSi60%, and CdS/PSi70% structures present photocurrents of 3.14, 4.63, 58.85, 590.40 and 204.88 µA, respectively at bias voltage of 9V, as illuminated by visible light (Fig. 8c). In addition, the highest photocurrent value is observed for CdS/PSi60% structure. However, the current measured in CdS/PSi70% structure was substantially greater than that of CdS/PSi60%, this suggests the possibility of defects formation within the CdS thin films attributed to the high porosity of the substrate. These defects may behave as recombination centers and consequently reduces the electronic transport.

In conclusion, the electrical characteristics of the produced CdS thin films can be influenced by the surface shape and porosity of the porous silicon substrate.

Successful synthesis of CdS thin films was achieved on glass, silicon, and mesoporous silicon substrates using the chemical bath method.

4. Conclusion

This work has made it possible to meet the objectives set concerning the effect of porosity of mesoporous silicon substrates on CdS thin films deposited by chemical bath deposition. Successful synthesis of CdS thin films was achieved on glass, silicon, and mesoporous silicon substrates using the chemical bath method. Variations in the porosity of the PSi substrate yield to CdS thin films with various morphologies. The impact of PSi porosity on the grain size of CdS was studied. Indeed, a porosity of around 70% yields to films owing better crystallinity and reduces the size of the CdS grains to less than 12 nm. The DC current measurements showed that the CdS/PSi structure with porosities between 60-70% significantly exhibited larger conductivity and photoconductivity, compared to the CdS/glass and CdS/Si structures. Finally, due to the vast complexity of the influence of the porosity of PSi substrate on the characteristics of CdS nanoparticles, several issues are still open for future investigation in order to fully understand the effect of porosity of silicon substrates on CdS thin films. Hopefully, the results presented in this study give a contribution to this understanding.

Acknowledgments

This research was funded by the DGRSDT and the laboratory of Materials and System Structure and their Reliability of Oum El Bouaghi University, Algeria.

References

[1] Y. Benkrima, D. Belfennache, R. Yekhlef, A. M. Ghaleb,Chalcogenide Lett. **20(8)**.609-618 (2023); https://doi.org/10.15251/CL.2023.208.609

[2] M. Husham, Z. Hassan, A .M. Selman. Eur. Phys. J. Appl. Phys. **74(1).** 10101 (2016);https://doi.org/10.1051/epjap/2016150414

[3] D. Belfennache, D. Madi, R. Yekhlef, L. Toukal, N. Maouche, M.S. Akhtar, S. Zahra. Semicond. Phys. Quantum Electron. Optoelectron.. **24(4)**.378-389 (2021) ;https://doi.org/10.15407/spqeo24.04.378

[4] S. Mahdid, D. Belfennache , D. Madi, M. Samah, R. Yekhlef, Y. Benkrima,. J. Ovonic. Res.**19(5).** 535-545 (2023); https://doi.org/10.15251/JOR.2023.195.535

[5] P. Priyadarshini, S. Das, R. Naik.RSC Advances **12(16)**. 9599–9620 (2022) ;https://doi.org/10.1039/D2RA00771A

[6] Y. Xi, C. Hu, C.Zheng, H. Zhang, R. Yang,Y. Tian, Mater. Res. Bull. **45(10).** 1476–1480 (2010) ;https://doi.org/10.1016/j.materresbull.2010.06.007

[7] J. Zhang, D. Li, R. Chen, Q. Xiong, Nature.**493(7433).** 504–508 (2013) ; https://doi.org/10.1038/nature11721

[8] D. Li, J. Zhang, Q. Zhang, Q. Xiong. Nano Lett.**12(6).** 2993–2999 (2012) ; https://doi.org/10.1021/nl300749z

[9] T. Zhai, X. Fang, L. Li, Y. Bando,D.Golberg, Nanoscale.**2(2),** 168–187 (2010).https://doi.org/10.1039/B9NR00415G

[10] H.Li, X. Wang, J. Xu, Q. Zhang, Y. Bando, D. Golberg, Y. Ma, T. Zhai, Adv. Mater.**25(22)**. 3017–3037 (2013) ; https://doi.org/10.1002/adma.201300244

[11] A. Ashok, G.Regmi, A. Romero-N´u˜nez, M. Solis-Lopez, S. Velumani, H. Castaneda,J. Mater. Sci. Mater. Electron. **31**. 7499–7518 (2020) ; https://doi.org/10.1007/s10854-020-03024-3

[12] S. Hariech,M. S. Aida,J. Bougdira,M.Belmahi, G. Medjahdi, D. Geneve, N. Attaf, H. Rinnert, J.Semicond.**39(3)**. 034004 (2018) ;https://doi.org/10.1088/1674-4926/39/3/034004

[13] H. Khallaf, Electronic Theses and Dissertations. 3941 (2009). https://stars.library.ucf.edu/etd/3941

[14] D. Belfennache, N. Brihi, D. Madi, Proceeding of the IEEE xplore, 8th (ICMIC) (2016). 7804164. 497–502 (2017). https://doi.org/10.1109/ICMIC.2016.7804164.

[15] D. Belfennache, D. Madi, N. Brihi, M. S. Aida, M. A. Saeed, Appl. Phys. A. **124**. 697 (2018). https://doi.org/10.1007/s00339-018-2118-z.

[16] R. Pribyl, S. Kelarova, M. Karkus, V. Bursikova, Carbon Trends, **17**.100416 (2024); https://doi.org/10.1016/j.cartre.2024.100416.

[17] T.A.-H. Abbas,Diyala journal for pure sciences.**13(3)**. 227-245 (2017) ;https://doi.org/10.24237/djps.1303.261A

[18] R. Ouldamer, D. Madi, D. Belfennache, In: Hatti, M. (eds) Advanced Computational Techniques for Renewable Energy Systems. IC-AIRES 2022. Lecture Notes in Networks and Systems, **591**, 700-705 (2023) Springer, Cham.; https://doi.org/10.1007/978-3-031-21216-1_71

[19] E. V. Pasos, B. Wagner, F. Xu, Y. Wang, M. Kim, M. Zachariah, L. Mangolini, Chem Eng J. **500**. 156997 (2024); https://doi.org/10.1016/j.cej.2024.156997.

[20] R. Ouldamer, D. Belfennache, D. Madi, R. Yekhlef, S. Zaiou, Mohamed A. Ali, J. Ovonic. Res. **20(1)**.45-55 (2024); https://doi.org/10.15251/JOR.2024.201.45

[21] N. Naderi, M. Hashim Int. J. Electrochem. Sci**7(11)**. 11512–11518 (2012) ; https://doi.org/10.1016/S1452-3981(23)16962-8

[22] I. González, R. Nava, M. Cruz-Irisson, J.A. del Río, I. Ornelas-Cruz, J. Pilo, Y.G. Rubo, A. Trejo, J. Tagüeña, J. Energy Storage. **102**. 114087 (2024);https://doi.org/10.1016/j.est.2024.114087.

[23] T. Jalkanen, A. Maattanen, E. Makila, et al. Journal of Sensors, 927396 (2015) ;https://doi.org/10.1155/2015/927396

[24] N.Rahmani, R. S. Dariani, AIPAdvances, **5**. 077112(2015) ;https://doi.org/10.1063/1.4926460.

[25] N.Rahmani, R. S.Dariani, M. Rajabi, Appl. Surf. Sci.**366**. 359–364 (2016)https://doi.org/10.1016/j.apsusc.2016.01.075.

[26] A .Halimaoui, Vial, JC., Derrien, J. (eds), Porous Silicon Science and Technology, Centre de Physique des Houches, Springer Berlin Heidelberg,**1**.33–52(1995) ;https://doi.org/10.1007/978-3-662-03120-9_3

[27] M.du Plessis,PhysicaStatusSolidi (a), **204(7)**.2319– 2328 (2007) ;https://doi.org/10.1002/pssa.200622237

[28] A. Rahmani, L. Remache, M. Guendouz, M. S. Aida, Z. Hebboul, Appl.Phys. A **127(5)**. 396 (2021) ;https://doi.org/10.1007/s00339-021-04548-z

[29] C-M. Chou, H-T. Cho, V. K. Hsiao, K-T.Yong, W-C. Law, Nanoscale Res. Lett. **7**. 1–4 (2012) ;https://doi.org/10.1186/1556-276X-7-291

[30] B. Meier, L. Egermann,S. Voigt, M.Stanel, H. Kempa, A. C. Huebler. Thin Solid Films **519(19)**. 6610–6612 (2011);https://doi.org/10.1016/j.tsf.2011.04.225

[31] S. A. Hasoon, I. M. Ibrahim, R. Al-Haddad, S. S. Mahmood, Int. J. Curr. Eng. Technol. **4(2)**, 594–601 (2014)

[32] S. T. Kassim, H. A. Hadi, R. A. Ismail, Optik**221**. 165339 (2020) ;https://doi.org/10.1016/j.ijleo.2020.165339

[33] K. S. Khashan, Int. J. Mod. Phys. B. **25**(02), 277–282 (2011) ;https://doi.org/10.1142/S0217979211054744

[34] N. F. Habubi, R.A. Ismail, A. N. Abd, W. K. Hamoudi, Indian J. Pure Appl. Phy. **53**, 718-724 (2015).

[35] Y. Li, X. Y. Song,Y. L. Song, P. F. Ji, F. Q. Zhou,M. L. Tian, H. C. Huang, X. J. Li, Mater. Res. Bull. **74**. 507–510 (2016) ; https://doi.org/10.1016/j.materresbull.2015.11.023

[36] P. M. Perillo, D. F. Rodriguez, Physica B: Condensed Matter, **680**. 415828 (2024) ;https://doi.org/10.1016/j.physb.2024.415828

[37] M. Cao, Y. Sun, J. Wu, X. Chen,N. Dai. J. Alloys Compd. **508(2)**. 297–300 (2010) ;https://doi.org/10.1016/j.jallcom.2010.08.066

[38] C. Tsai, D. Chuu, G. Chen, S. Yang. J.Appl. Phys. **79(12)**, 9105–9109 (1996) ;https://doi.org/10.1063/1.362645

[39] B-S. Moon, J-H. Lee, H. Jung. Thin solid films **511**. 299–303 (2006) ;https://doi.org/10.1016/j.tsf.2005.11.080

[40] D. W. Niles, H. H¨ochst, Phys. Rev. B **41**(18), 12710 (1990) ;https://doi.org/10.1103/PhysRevB.41.12710

[41] J. Patel, F. Mighri, A. Ajji, D. Tiwari, T. K. Chaudhuri, Appl.Phys. A **117**.1791–1799 (2014)https://doi.org/10.1007/s00339-014-8659-x

[42] M. Cao, L.Li,B. Zhang, J. Huang, K. Tang, H. Cao, Y. Sun, Y. Shen,J. Alloys Compd. **530**. 81–84 (2012) ;https://doi.org/10.1016/j.jallcom.2012.03.054

[43] Z. Rabeel, M. Abbas, M. Basit, N. A. Shah, I. Ahmad, M. Hassan, J. Adv Nanomat**2(2)**. 113 (2017) ;https://dx.doi.org/10.22606/jan.2017.22004

[44] S. A-J. Jassim, A. A. R. A. Zumaila, G. A. A. Al Waly, Results Phys **3**.173–178 (2013) ;https://doi.org/10.1016/j.rinp.2013.08.003

[45] S. E. Haque, B. Ramdas, N. Padmavathy, A. SheelaMicro & Nano Letters**9(10)**. 731–735 (2014) ; https://doi.org/10.1049/mnl.2014.0167

[46] L. Ma, X. Ai, X. Wu, J.Alloys.Compd.**691**. 399–406 (2017) ;https://doi.org/10.1016/j.jallcom.2016.08.298

[47] S. Thanikaikarasan,T. Mahalingam, T. Ahamad, S. M. AlshehriJ. Saudi Chem. Soc.**24(12)**. 955–962 (2020) ;https://doi.org/10.1016/j.jscs.2020.10.003

[48] N.Maticiuc, J.Hiie. IOP Conf. Ser.: Mater. Sci. Eng.**49(1)**.012061(2013) ;https://doi.org/10.1088/1757-899X/49/1/012061

[49] F. Ouachtari, A.Rmili, B. Elidrissi, A. Bouaoud, H. Erguig, P. Elies, J. Mod. Phys.**2(9)**, 1073-1082(2011) ; https://doi.org/10.4236/jmp.2011.29131

[50] V. G. Nair,R. Jayakrishnan,J. John, J. A. Salam, A. M. Anand, A. Raj, Mater. Chem. Phys. **247**, 122849 (2020). https://doi.org/10.1016/j.matchemphys.2020.122849

[51] I. Horcas, R. Fernández, J.M. Gomez-Rodriguez, J. Colchero; J. Gómez-Herrero; A. M. Baro, Rev. Sci. Instrum. **78(1)**. 013705 (2007) . https://doi.org/10.1063/1.2432410

[52] R.A. Ismail, A.M E. Al-Samarai, A. Y. Ali, Optik, **168**. 302-312 (2018). https://doi.org/10.1016/j.ijleo.2018.04.101.

[53] D. Komaraiah, E. Radha, Y. Vijayakumar, J. Sivakumar, M. R. Reddy,R. Sayanna, Modern Research in Catalysis**5(4)**. 130–146 (2016) ;https://doi.org/10.4236/mrc.2016.54011

[54] M. Shaban, M. Mustafa, A. El Sayed, Mater. Sci. Semicond. Process. **56**. 329–343 (2016)https://doi.org/10.1016/j.mssp.2016.09.006

[55] G. Mani, J. B. B. Rayappan, Appl. Surf. Sci. **311**. 405–412 (2014)https://doi.org/10.1016/j.apsusc.2014.05.075